Stochastic Variational Approach to Small Atoms and Molecules Coupled to Quantum Field Modes in Cavity QED

Alexander Ahrens,[1] Chenhang Huang,[1] Matt Beutel,[1] Cody Covington,[2] and Kálmán Varga[1,*]
[1]Department of Physics and Astronomy, Vanderbilt University, Nashville, Tennessee 37235, USA
[2]Department of Chemistry, Austin Peay State University, Clarksville, Tennessee 37044, USA

(Received 24 August 2021; accepted 2 December 2021; published 27 December 2021)

In this work, we present a stochastic variational calculation (SVM) of energies and wave functions of few particle systems coupled to quantum fields in cavity QED. The spatial wave function and the photon spaces are optimized by a random selection process. Using correlated basis functions, the SVM approach solves the problem accurately and opens the way to the same precision that is reached the nonlight coupled quantum systems. Examples for a two-dimensional trion and confined electrons as well as for the He atom and the H_2 molecule are presented showing that the light-matter coupling drastically changes the electronic states.

DOI: 10.1103/PhysRevLett.127.273601

Strong coupling of cavity electromagnetic modes and molecules creates hybrid light-matter states modifying potential energy surfaces, charge states, and electronic structure. The possibility of altering physical and chemical properties by coupling to light attracted intense experimental [1–12] and theoretical interest [13–49]. The experimental investigations are overarching exciton transport [1,3], polariton condensation [2,9], transfer of excitation [6], and chemical reactivity [50]. The theoretical works explored excitation and charge transfer [20], self-polarization [36], potential energy surfaces [24] electron transfer [38], excitons [27], ionization potentials [34], and intermolecular interactions [35] in cavities, to name a few.

For atoms and molecules in a vacuum, high precision measurements and theoretical calculations have been developed. The accuracy of theoretical prediction [51] and experimental measurement [52] reaches the level of 1 MHz for the dissociation energy of the H_2 molecule. The theoretical description of the light-matter states is far from this accuracy. The main reason behind this is that the accurate wave function methods developed in quantum chemistry are computationally expensive even before an additional degree of freedom (light) is added, and the density functional theory [53] calculations lack suitable functionals for light-matter coupling. Initial developments have been started in both directions [19,22,26,32,34,37].

In this work, we use the stochastic variational calculation (SVM) to build optimized light-matter coupled wave function (WF). By selecting the best light-matter coupled basis states, the SVM produces highly accurate energies and WFs. The precision can reach the same level as the conventional nonlight-coupled quantum chemistry calculations. The stochastic selection keeps the basis dimension and the computational cost manageable by avoiding the high-dimensional tensor product spaces. The SVM works for strong coupling and can go beyond a single photon mode using correlated basis functions, while other approaches are limited to very weak couplings, a single photon mode, or use mean-field or model Hamiltonians.

We will show that the light-matter coupled WFs are drastically different from the noncoupled electronic WFs and the emerging features cannot be explained by the electronic plus the dipole self-interaction Hamiltonian (that acts on the spatial part of the WF) alone. The WF components in different photon subspaces are very different showing well-separated density peaks in systems that were spherically symmetric before coupling to light. By changing the coupling strength or adding more than one photon modes a certain subspace can be dominant and these exotic density distributions might be experimentally observable.

The spatial WFs will be represented by explicitly correlated Gaussian (ECG) basis functions [54]. The advantage of the approach is that the matrix elements are analytically available [55–57] and it allows very accurate calculations of energies and WFs [54,58–63].

We assume that the system is nonrelativistic and the coupling to the light can be described by the dipole approximation. The Pauli-Fierz (PF) nonrelativistic QED Hamiltonian provides a consistent quantum description at this level [21,25,38,46,64]. The dipole approximation assumes that the spatial variation of the electric field is negligible across the size of the system, and this is valid if the system size is much smaller than the wavelength of the light. The PF Hamiltonian in the Coulomb gauge is $H = H_e + H_{ep}$ where H_e is the electronic Hamiltonian and

$$H_{ep} = \sum_{\alpha=1}^{N_p} \left[\omega_\alpha \left(\hat{a}_\alpha^+ \hat{a}_\alpha + \frac{1}{2} \right) - \omega_\alpha q_\alpha \vec{\lambda}_\alpha \vec{D} + \frac{1}{2} (\vec{\lambda}_\alpha \vec{D})^2 \right], \quad (1)$$

(atomic units are used in this work). In Eq. (1) $\vec{D}$ is the dipole operator, the photon fields are described by

quantized oscillators, and $q_\alpha = (1/\sqrt{2\omega_\alpha})(\hat{a}_\alpha^+ + \hat{a}_\alpha)$ is the displacement field. This Hamiltonian describes N_p photon modes with photon frequency ω_α and coupling $\vec{\lambda}_\alpha$. The coupling term is written as [65] $\vec{\lambda}_\alpha = \sqrt{4\pi} S_\alpha(\vec{r})\vec{e}_\alpha$, where $S_\alpha(\vec{r})$ is the cavity mode function at $\vec{r}$ and $\vec{e}_\alpha$ is the transversal polarization vector of the photon. The first term in Eq. (1) is the Hamiltonian of the photon modes, the second term couples the photons to the dipole, and the last term is the dipole self-interaction, $H_d = \frac{1}{2}\sum_{\alpha=1}^{N_p}(\vec{\lambda}_\alpha \vec{D})^2$.

The Hamiltonian of an N electron system confined in an external potential V_c is

$$H_e = -\sum_{i=1}^{N}\frac{\nabla_i^2}{2m_i} + \sum_{i<j}^{N}\frac{q_i q_j}{|\mathbf{r}_i - \mathbf{r}_j|} + \sum_{i=1}^{N} V_c(\mathbf{r}_i), \quad (2)$$

where $\mathbf{r}_i$, q_i, and m_i are the coordinate, charge, and mass of the ith particle.

Introducing the notations $\vec{r} = (\mathbf{r}_1, \ldots, \mathbf{r}_N)$, and $|\vec{n}\rangle = |n_1\rangle|n_2\rangle, \ldots, |n_{N_p}\rangle$ where n_α is the number of photons in mode α, the variational WF is written as a linear combination of products of spatial and photon basis functions

$$\Psi(\vec{r}) = \sum_{\vec{n}}\sum_{k=1}^{K_{\vec{n}}} c_k^{\vec{n}} \psi_k^{\vec{n}}(\vec{r})|\vec{n}\rangle. \quad (3)$$

The spatial part of the WF is expanded into ECGs for each photon state $|\vec{n}\rangle$ as

$$\psi_k^{\vec{n}}(\vec{r}) = \mathcal{A}\{e^{-\frac{1}{2}\sum_{i<j}^{N}\alpha_{ij}^k(\mathbf{r}_i-\mathbf{r}_j)^2 - \frac{1}{2}\sum_{i=1}^{N}\beta_i^k(\mathbf{r}_i-\mathbf{s}_i^k)^2}\Lambda(\vec{r})\chi_S\} \quad (4)$$

where $\mathcal{A}$ is an antisymmetrizer, χ_S is the N electron spin function (coupling the spin to S), and α_{ij}^k, β_i^k, and $\mathbf{s}_i^k$ are nonlinear parameters.

The dipole self-interaction introduces a nonspherical term into the Hamiltonian. The solution of this nonspherical problem is difficult and slowly converging using angular expansions. We introduce $\Lambda(\vec{r}) = e^{\vec{r}U\vec{r}}$ in Eq. (4) to eliminate the dipole self-interaction term H_d from Eq. (1). U is a $3N \times 3N$ matrix with elements chosen to cancel the dipole self-energy [66]. The matrix elements can be analytically calculated for both the spatial [54,55] and the photon parts and the Hamiltonian and overlap matrices are very sparse matrices [66].

We will optimize the basis functions selecting the best spatial basis parameters and photon components using the SVM. In the SVM, the basis functions are optimized by randomly generating a large number of candidates and selecting the ones that give the lowest energy [54,55,67]. The size of the basis can be increased by adding the best states one by one and a K-dimensional basis can be refined by replacing states with randomly selected better basis functions. The details of the SVM selection are given in [66].

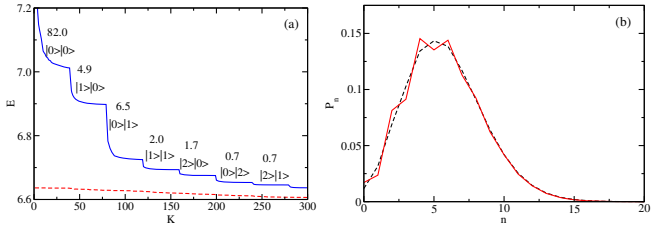

FIG. 1. (a) Energy convergence of the SVM calculation. (b) Photon space occupations for the ground state with $\vec{\lambda} = (0.5, 0.5)$ a.u., solid line: SVM, dashed line: exact diagonalization.

In Fig. 1(a) we show an example for the energy convergence of a two-dimensional trion (two electrons and a hole) coupled to two photon modes using the SVM with $K_{\vec{n}} = 40$ basis vectors in each photon state. Initially the photon space $|n_1\rangle|n_2\rangle$ is restricted by $n_1 + n_2 < 4$. First the $|0\rangle|0\rangle$ space is optimized by adding basis functions selected by the SVM one by one. Then the $|1\rangle|0\rangle$ space is added and populated by the SVM and this process is repeated for each allowed photon space. The energy quickly converges in the photon spaces and the energy gain is less and less as higher photon numbers are added. Next, the WF is optimized further with a refining step [66], where the basis is improved by randomly replacing photon spaces with energetically more favorable ones. In this step, the photons can also couple photon spaces with $n_1 + n_2 \geq 4$. As the dashed line in Fig. 1(a) shows, this step significantly improves the energy.

To test the accuracy of the approach we have compared the converged energies to a one-electron one-photon problem which can be solved numerically [22,40,41]. The SVM and exact diagonalization energies agree up to five digits for the lowest five states [66]. Figure 1(b) shows photon occupations for a very strong coupling case. The SVM and the exact diagonalization results are in very good agreement.

We use a harmonically confined ($V_c(r) = \frac{1}{2}\omega_c^2 r^2$) two-dimensional (2D) two-electron system coupled to two photon modes as a second test case, because this problem is analytically solvable [68]. Using $\omega_c = 1$ a.u. for the harmonic confinement, $\omega_1 = 1$, $\omega_2 = 1$ a.u. for the photon frequencies, and $\vec{\lambda}_1 = (1, 1)$, $\vec{\lambda}_2 = (-1, -1)$ a.u. for the coupling, the exact energy of the system is $E = 3.654\,00$ a.u. This choice corresponds to a diagonally polarized light and mode functions $S_\alpha(\vec{r}) = \sqrt{(2/AL)}\sin(k_\alpha x)$ where L is the length, AL is the volume of the cavity, and $k_\alpha = \alpha\pi/L$ is the wave vector ($\alpha = 1, 2$). Our system is placed at the center of the cavity, $x = L/2$ and $\vec{\lambda}_2 = -\vec{\lambda}_1$. The calculated energy $E = 3.654\,01$ a.u. is in perfect agreement with the analytical value and the photon space probabilities also agree [66].

Next we study a 2D three electron system in harmonic confinement ($\omega_c = 1/3$ a.u.) coupled to photon mode of

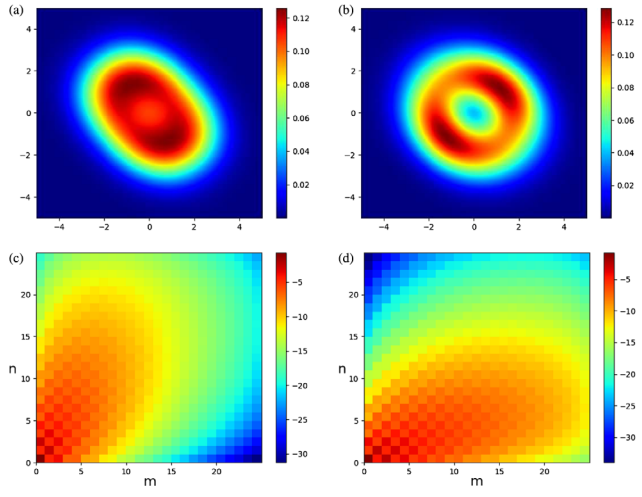

FIG. 2. Electron density of a harmonically confined 2D three-electron system ($\omega = 2$ and $\lambda = 4$) (a) $S = 1/24$, (b) $S = 3/2$. Photon distribution (logarithm of the occupation probability) for two photons modes in the 2D three-electron system, $S = 1/2$, $\omega_1 = 1/2\omega_2 = 1$; (c) $\vec{\lambda}_1 = (5, 5)$, $\vec{\lambda}_2 = (-5, -5)$, (d) $\vec{\lambda}_1 = (5, 5)$, $\vec{\lambda}_2 = (-10, -10)$. n is the number of photons in the ω_1 mode and m is the number of photons in the ω_2 mode.

$\omega_1 = 2$ and $\vec{\lambda}_1 = (4, 4)$. Without coupling to the light the electron density of these systems is spherically symmetric. The $S = 1/2$ density has a peak in the center, while the $S = 3/2$ system forms a ringlike structure due to the Pauli repulsion between the spin-polarized electrons [66]. The electron density is shown in Fig. 2 for $S = 1/2$ and $S = 3/2$ with a very different structure for the coupled case. The density peak in the $S = 1/2$ case breaks up into two peaks and the $S = 3/2$ ring also splits into two parts. This shows how strongly the light-matter coupling can change the electron density of the system. Figures 2(c) and 2(d) show the photon distribution for this system when it is coupled to two photon modes. When the coupling strength of the two modes are equal then the lower frequency mode (ω_1) is more occupied [Fig. 2(c)] because more photons are needed to couple the energy levels. The checkerboard structure is explained by the dependence of the coupling strengths on the parity of the sum of the photon numbers in the two modes (if n is the number of photons in ω_1 and m is the number of photons in ω_2 mode, then $n + m$ is even or odd). By increasing the coupling strength of the second mode (ω_2) the occupations can be changed and the photon occupations will be higher in ω_2 than in ω_1 [Fig. 2(d)]. Photon states with very small occupations ($< 10^{-10}$) do not significantly contribute to the energy and structure of the system.

The next example is a trion [69–72], two electrons and a hole in 2D coupled to a one-photon mode and two-photon modes. The electron densities of the trion coupled to one- and two-photon modes are shown in Figs. 3 and 4. The figures show the density

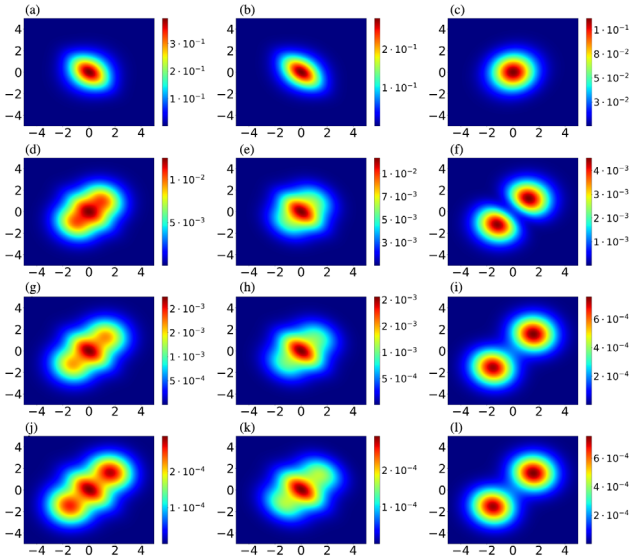

FIG. 3. Two electrons and a hole in 2D coupled to one photon mode [$\omega_1 = 2$, $\vec{\lambda}_1 = (4, 4)$ a.u.]. The left column [(a), (d), (g), (j)] shows the total single particle density; the electron density is in the middle [(b), (e), (h), (k)]; and the right column [(c), (f), (i), (l)] shows the density of the hole. The first row belongs to the photon space $|0\rangle$, the second to $|1\rangle$, the third to $|2\rangle$, and the fourth to $|3\rangle$. The x axis is the horizontal, the y axis is the vertical direction.

$$\rho_{\vec{n}}(\vec{r}) = \sum_{i=1}^{3} \sum_{j,k=1}^{K_{\vec{n}}} c_j^{\vec{n}} c_k^{\vec{n}} \langle \psi_j^{\vec{n}} | \delta(\mathbf{r}_i - \mathbf{r}) | \psi_k^{\vec{n}} \rangle \tag{5}$$

belonging to photon state $\vec{n}$ and we also show the contribution of the electrons and hole to the density.

Figures 3(a) and 4(b) show the density in the $|0\rangle$ and the $|0\rangle|0\rangle$ photon spaces. The total densities are very similar to these densities because the $|0\rangle$ and $|0\rangle|0\rangle$ photon spaces are dominant (92% and 82% of the wave function belong to these states). The weights of WF components in photon spaces depend on the frequency and coupling, and by changing these, other photon states (or linear combinations

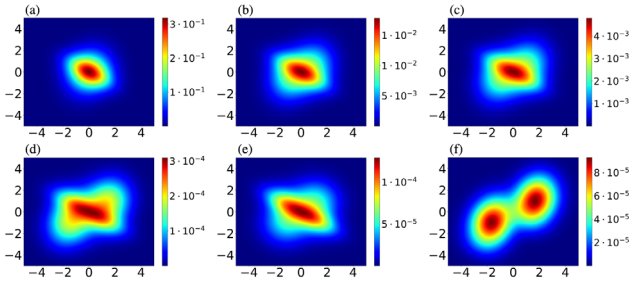

FIG. 4. Two electrons and a hole in 2D coupled to two photon modes [$\omega_1 = 2$, $\omega_2 = 4$, $\vec{\lambda}_1 = (4, 4)$, $\vec{\lambda}_2 = (-4, -4)$ a.u.] The total single particle densities in photon space $|0\rangle|0\rangle$ (a), $|1\rangle|0\rangle$ (b), $|1\rangle|1\rangle$ (c), $|2\rangle|2\rangle$ (d). The electron density in $|2\rangle|2\rangle$ (e) and the hole density in $|2\rangle|2\rangle$ (f) are also shown. The x axis is the horizontal, the y axis is the vertical direction.

of photon states) become major contributors to the density. The total densities are very similar to each other in the one- and two-photon mode coupled cases [Figs. 3(a) and 4(b)]; they are slightly squeezed along the $x = -y$ diagonal axis.

Figures 3(b) and 3(c) show the electron and hole density of the trion in the $|0\rangle$ photon space. The hole density is circularly symmetric, the electron density is elongated and the superposition of these two explains the structure seen in Fig. 3(a). In the $|1\rangle$ photon space the density is elongated [Fig. 3(d)] but now it is aligned in the direction of the $x = y$ diagonal. This density is a superposition of two outside hole peaks [Fig. 3(f)] and an electron in the middle [Fig. 3(e)]. The $|2\rangle$ and $|3\rangle$ photon spaces are similar [Fig. 3(g)]. The electron density not only has a peak in the middle but also a bondlike structure toward the hole peaks. The $|3\rangle$ photon space densities [Figs. 3(j), 3(k), and 3(l)] are similar to the $|0\rangle$ ones, but now the total density has three separate peaks.

In the trion coupled to the two-photon mode case (Fig. 4) we keep ω_1 and $\vec{\lambda}_1$ the same as before and add a second photon mode with $\omega_2 = 2\omega_1$ and $\vec{\lambda}_2 = -\vec{\lambda}_1$. The second mode has stronger coupling because the frequency is larger. We still see gradual elongation in higher photon spaces, but the densities are quite different from the one-photon mode case. The resulted linear combinations are shown in Figs. 4(b), 4(c), and 4(d). The underlying electron and hole densities still show somewhat similar structures to the one-photon mode. For example, the total density in the $|2\rangle|2\rangle$ photon space [Fig. 4(d)] is the sum of the electron density in the middle [Fig. 4(e)] and the two peaks of the hole [Fig. 4(f)] outside.

Next, we study the energy as a function of the distance between the nuclei in a three-dimensional H_2 molecule coupled to one- and two-photon modes. In this case, two protons are fixed at a distance r and the energy is calculated as a function of r. We have studied four cases, the four energy curves, together with the ground state energy curve are shown in Fig. 5(a). The energy of the system shifts up by coupling to light, and the energy shifts higher when the $\vec{\lambda}$ coupling is larger. The effect of ω (not shown in the figure) is much smaller. The shift in the two-photon mode case is much larger because now two dipole self-interaction terms increase the energy. The most interesting result is that by increasing $\vec{\lambda}$ the energy minimum moves to much shorter distances.

The last example is a spin singlet He atom with finite nuclear mass [73,74] coupled to a single photon mode. Figure 5(b) shows the lowest energy levels as a function of $\vec{\lambda} = (\lambda, \lambda, 0)$ for $\omega = 0.8$ a.u. Besides the bound S, P, and D states of the He atom, discretized continuum states are also included for $\lambda = 0$. The thick line shows the energy of the dissociation threshold into He^+ ion plus an electron. Figure 5(b) shows that even some continuum states will become bound as λ increases. The figure also shows that

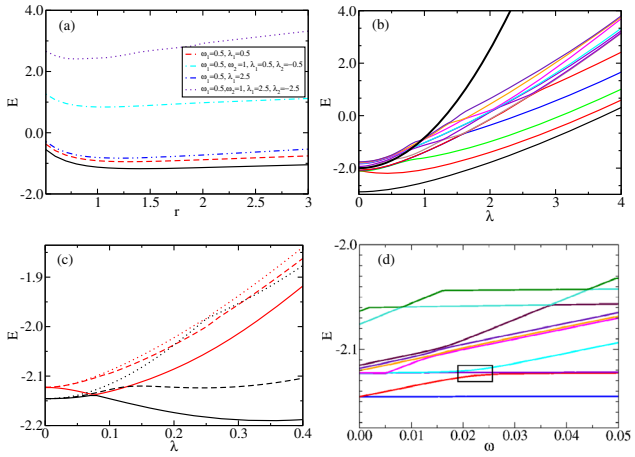

FIG. 5. (a) Ground state energy of H_2 as a function of bond length (solid line) and energies of the H_2 molecule coupled to light. $\vec{\lambda}_i = \lambda_i(1, 1, 0)$. (b) Energy of the lowest lying states of He as a function of λ for $\omega = 0.8$ a.u. (c) Energy of the 2^1S^e (starts at -2.14 a.u.) and 2^1P^o (starts at -2.12 a.u.) as a function of λ, for $\omega = 0.8$ a.u. (solid lines), $\omega = 0.4$ a.u. (dashed lines) and $\omega = 0.2$ a.u. (dotted lines). (d) Energy of states lying around the 2^1S^e and 2^1P^o as a function of ω ($\sqrt{\omega}/\lambda$ is kept constant).

certain energy levels get very close to each other and then they move away (avoided crossing). This energy level repulsion is due to the fact that changing λ modifies the potential shape which, in turn, drives up or down energy levels but no degeneracy is introduced and the energy levels cannot cross each other.

The role of ω is illustrated [see Fig. 5(c)] for the 2^1S^e and 2^1P^o energy levels. For $\omega = 0.8$ a.u., the 2^1P^o state moves down, approaching the 2^1S^e level at around $\lambda = 0.08$ a.u., and then it moves up while the energy of the other state decreases [and later increases as Fig. 5(b) shows]. In the case of $\omega = 0.4$ a.u. the 2^1S^e state moves up but the closest distance between the two states (at around $\lambda = 0.12$ a.u.) is much larger than the size of the previous gap. In the $\omega = 0.2$ a.u. case the two curves meet at $\lambda = 0.27$ a.u. These examples show that ω strongly influences the position of the avoided crossing points and it also affects the rise of the energy curves.

Figure 5(d) shows the energy levels at an even lower coupling strength. In this case we have changed ω keeping $\sqrt{\omega}/\lambda = 23.45$ fixed. In this way at $\omega = E_{2^1S^e} - E_{2^1P^o} = 0.22$ a.u. λ is 0.02 a.u. and the coupling strength is proportional to ω as suggested in Ref. [42] to mimic the Jaynes-Cummings model [75]. The box in the middle of Fig. 5(d) shows the position where the 2^1S^e and 2^1P^o state get close to each other at around the $\omega = 0.22$ a.u. transition energy and at that point the energy difference between them is 0.0055 a.u., which corresponds to a Rabi splitting of 0.1496 eV in excellent agreement with the real space grid based calculation (0.148 eV) in Ref. [42].

This work has been supported by the National Science Foundation (NSF) under Grant No. IRES 1826917.

A. A., C. H., and M. B. equally contributed to this work.

*kalman.varga@vanderbilt.edu

[1] J. Feist and F. J. Garcia-Vidal, Phys. Rev. Lett. **114**, 196402 (2015).
[2] R. Balili, V. Hartwell, D. Snoke, L. Pfeiffer, and K. West, Science **316**, 1007 (2007).
[3] J. Schachenmayer, C. Genes, E. Tignone, and G. Pupillo, Phys. Rev. Lett. **114**, 196403 (2015).
[4] B. Xiang, R. F. Ribeiro, M. Du, L. Chen, Z. Yang, J. Wang, J. Yuen-Zhou, and W. Xiong, Science **368**, 665 (2020).
[5] A. Reserbat-Plantey, I. Epstein, I. Torre, A. T. Costa, P. A. D. Gonalves, N. A. Mortensen, M. Polini, J. C. W. Song, N. M. R. Peres, and F. H. L. Koppens, ACS Photonics **8**, 85 (2021).
[6] D. M. Coles, N. Somaschi, P. Michetti, C. Clark, P. G. Lagoudakis, P. G. Savvidis, and D. G. Lidzey, Nat. Mater. **13**, 712 (2014).
[7] J. Kasprzak *et al.*, Nature (London) **443**, 409 (2006).
[8] T. Schwartz, J. A. Hutchison, C. Genet, and T. W. Ebbesen, Phys. Rev. Lett. **106**, 196405 (2011).
[9] J. D. Plumhof, T. Stöferle, L. Mai, U. Scherf, and R. F. Mahrt, Nat. Mater. **13**, 247 (2014).
[10] J. A. Hutchison, A. Liscio, T. Schwartz, A. Canaguier-Durand, C. Genet, V. Palermo, P. Samor, and T. W. Ebbesen, Adv. Mater. **25**, 2481 (2013).
[11] K. Wang, M. Seidel, K. Nagarajan, T. Chervy, C. Genet, and T. Ebbesen, Nat. Commun. **12**, 1486 (2021).
[12] D. N. Basov, A. Asenjo-Garcia, P. J. Schuck, X. Zhu, and A. Rubio, Nanophotonics **10**, 549 (2021).
[13] G. Mazza and A. Georges, Phys. Rev. Lett. **122**, 017401 (2019).
[14] O. Di Stefano, A. Settineri, V. Macrì, L. Garziano, R. Stassi, S. Savasta, and F. Nori, Nat. Phys. **15**, 803 (2019).
[15] J. Galego, F. J. Garcia-Vidal, and J. Feist, Phys. Rev. X **5**, 041022 (2015).
[16] F. Herrera and F. C. Spano, Phys. Rev. Lett. **116**, 238301 (2016).
[17] J. Galego, F. J. Garcia-Vidal, and J. Feist, Nat. Commun. **7**, 13841 (2016).
[18] A. Shalabney, J. George, J. Hutchison, G. Pupillo, C. Genet, and T. W. Ebbesen, Nat. Commun. **6**, 5981 (2015).
[19] F. Buchholz, I. Theophilou, S. E. B. Nielsen, M. Ruggenthaler, and A. Rubio, ACS Photonics **6**, 2694 (2019).
[20] C. Schäfer, M. Ruggenthaler, H. Appel, and A. Rubio, Proc. Natl. Acad. Sci. U.S.A. **116**, 4883 (2019).
[21] M. Ruggenthaler, N. Tancogne-Dejean, J. Flick, H. Appel, and A. Rubio, Nat. Rev. Chem. **2**, 0118 (2018).
[22] J. Flick, M. Ruggenthaler, H. Appel, and A. Rubio, Proc. Natl. Acad. Sci. U.S.A. **112**, 15285 (2015).
[23] J. Flick, M. Ruggenthaler, H. Appel, and A. Rubio, Proc. Natl. Acad. Sci. U.S.A. **114**, 3026 (2017).
[24] L. Lacombe, N. M. Hoffmann, and N. T. Maitra, Phys. Rev. Lett. **123**, 083201 (2019).
[25] A. Mandal, S. Montillo Vega, and P. Huo, J. Phys. Chem. Lett. **11**, 9215 (2020).
[26] J. Flick, D. M. Welakuh, M. Ruggenthaler, H. Appel, and A. Rubio, ACS Photonics **6**, 2757 (2019).
[27] S. Latini, E. Ronca, U. De Giovannini, H. Hbener, and A. Rubio, Nano Lett. **19**, 3473 (2019).
[28] J. Flick, N. Rivera, and P. Narang, Nanophotonics **7**, 1479 (2018).
[29] J. Flick and P. Narang, Phys. Rev. Lett. **121**, 113002 (2018).
[30] F. J. Garcia-Vidal, C. Ciuti, and T. W. Ebbesen, Science **373**, eabd0336 (2021).
[31] A. Thomas *et al.*, Science **363**, 615 (2019).
[32] U. Mordovina, C. Bungey, H. Appel, P. J. Knowles, A. Rubio, and F. R. Manby, Phys. Rev. Research **2**, 023262 (2020).
[33] D. S. Wang, T. Neuman, J. Flick, and P. Narang, J. Chem. Phys. **154**, 104109 (2021).
[34] A. E. DePrince, J. Chem. Phys. **154**, 094112 (2021).
[35] T. S. Haugland, C. Schfer, E. Ronca, A. Rubio, and H. Koch, J. Chem. Phys. **154**, 094113 (2021).
[36] N. M. Hoffmann, L. Lacombe, A. Rubio, and N. T. Maitra, J. Chem. Phys. **153**, 104103 (2020).
[37] J. Flick and P. Narang, J. Chem. Phys. **153**, 094116 (2020).
[38] A. Mandal, T. D. Krauss, and P. Huo, J. Phys. Chem. B **124**, 6321 (2020).
[39] J. Galego, F. J. Garcia-Vidal, and J. Feist, Phys. Rev. Lett. **119**, 136001 (2017).
[40] J. Flick, C. Schfer, M. Ruggenthaler, H. Appel, and A. Rubio, ACS Photonics **5**, 992 (2018).
[41] C. Schafer, M. Ruggenthaler, and A. Rubio, Phys. Rev. A **98**, 043801 (2018).
[42] D. Sidler, M. Ruggenthaler, H. Appel, and A. Rubio, J. Phys. Chem. Lett. **11**, 7525 (2020).
[43] I. Theophilou, M. Penz, M. Ruggenthaler, and A. Rubio, J. Chem. Theory Comput. **16**, 6236 (2020).
[44] D. Sidler, C. Schfer, M. Ruggenthaler, and A. Rubio, J. Phys. Chem. Lett. **12**, 508 (2021).
[45] F. Buchholz, I. Theophilou, K. J. H. Giesbertz, M. Ruggenthaler, and A. Rubio, J. Chem. Theory Comput. **16**, 5601 (2020).
[46] I. V. Tokatly, Phys. Rev. B **98**, 235123 (2018).
[47] N. Rivera, J. Flick, and P. Narang, Phys. Rev. Lett. **122**, 193603 (2019).
[48] T. Szidarovszky, G. J. Halász, and Á. Vibók, New J. Phys. **22**, 053001 (2020).
[49] L. S. Cederbaum, J. Phys. Chem. Lett. **12**, 6056 (2021).
[50] A. Thomas *et al.*, Angew. Chem., Int. Ed. Engl. **55**, 11462 (2016).
[51] M. Puchalski, J. Komasa, P. Czachorowski, and K. Pachucki, Phys. Rev. Lett. **122**, 103003 (2019).
[52] N. Hölsch, M. Beyer, E. J. Salumbides, K. S. E. Eikema, W. Ubachs, C. Jungen, and F. Merkt, Phys. Rev. Lett. **122**, 103002 (2019).
[53] W. Kohn and L. J. Sham, Phys. Rev. **140**, A1133 (1965).
[54] J. Mitroy, S. Bubin, W. Horiuchi, Y. Suzuki, L. Adamowicz, W. Cencek, K. Szalewicz, J. Komasa, D. Blume, and K. Varga, Rev. Mod. Phys. **85**, 693 (2013).
[55] Y. Suzuki and K. Varga, *Stochastic Variational Approach to Quantum-Mechanical Few-Body Problems*, vol. 54 (Springer Science & Business Media, New York, 1998).
[56] J. Cioslowski and K. Strasburger, J. Chem. Phys. **146**, 044308 (2017).

[57] T. Zaklama, D. Zhang, K. Rowan, L. Schatzki, Y. Suzuki, and K. Varga, Few-Body Syst. **61**, 6 (2020).
[58] D. K. Zhang, D. W. Kidd, and K. Varga, Nano Lett. **15**, 7002 (2015).
[59] D. W. Kidd, D. K. Zhang, and K. Varga, Phys. Rev. B **93**, 125423 (2016).
[60] C. Riva, F. M. Peeters, and K. Varga, Phys. Rev. B **61**, 13873 (2000).
[61] K. Varga, Phys. Rev. Lett. **83**, 5471 (1999).
[62] J. Usukura, Y. Suzuki, and K. Varga, Phys. Rev. B **59**, 5652 (1999).
[63] K. Varga, P. Navratil, J. Usukura, and Y. Suzuki, Phys. Rev. B **63**, 205308 (2001).
[64] V. Rokaj, D. M. Welakuh, M. Ruggenthaler, and A. Rubio, J. Phys. B **51**, 034005 (2018).
[65] M. Ruggenthaler, J. Flick, C. Pellegrini, H. Appel, I. V. Tokatly, and A. Rubio, Phys. Rev. A **90**, 012508 (2014).
[66] See Supplemental Material at http://link.aps.org/supplemental/10.1103/PhysRevLett.127.273601 for additional details of the calculations.
[67] V. I. Kukulin and V. M. Krasnopol'sky, J. Phys. G **3**, 795 (1977).
[68] C. Huang, A. Ahrens, M. Beutel, and K. Varga, Phys. Rev. B **104**, 165147 (2021).
[69] R. P. A. Emmanuele *et al.*, Nat. Commun. **11**, 3589 (2020).
[70] S. Dhara, C. Chakraborty, K. M. Goodfellow, L. Qiu, T. A. O'Loughlin, G. W. Wicks, S. Bhattacharjee, and A. N. Vamivakas, Nat. Phys. **14**, 130 (2018).
[71] S. Dufferwiel *et al.*, Nat. Photonics **11**, 497 (2017).
[72] M. Sidler, P. Back, O. Cotlet, A. Srivastava, T. Fink, M. Kroner, E. Demler, and A. Imamoglu, Nat. Phys. **13**, 255 (2017).
[73] M. Hesse and D. Baye, J. Phys. B **34**, 1425 (2001).
[74] G. W. F. Drake and Z.-C. Yan, Phys. Rev. A **46**, 2378 (1992).
[75] E. Jaynes and F. Cummings, Proc. IEEE **51**, 89 (1963).